Letters on Materials 15 (4), 2025 pp. 284-289 www.lettersonmaterials.com

Received 5 August 2025; Accepted 17 October 2025 https://elibrary.ru/hgfaxq
https://doi.org/10.48612/letters/2025-4-284-289

Features of consolidation of hybrid layered amorphous-nanocrystalline Cu/FeSiB/Cu material by severe plastic deformation

R. V. Sundeev[†1,2,3], A. V. Shalimova[2], S. O. Rogachev[4,5], V. E. Bazhenov[4], G. K. Sultanova[6,7], O. P. Chernogorova[5]

[†]sundeev55@yandex.ru

[1]"MIREA — Russian Technological University", Moscow 119454, Russia
[2]I. P. Bardin Science Institute for Ferrous Metallurgy, Moscow 105005, Russia
[3]Institute for Electrophysics and Electric Power of the Russian Academy of Sciences, Moscow 119334, Russia
[4]National University of Science and Technology MISIS, Moscow 119049, Russia
[5]Baikov Institute of Metallurgy and Materials Science, RAS, Moscow 119334, Russia
[6]NRC "Kurchatov Institute" — TISNCM, Moscow, Troitsk 108840, Russia
[7]Moscow Institute of Physics and Technology (National Research University), Dolgoprudny 141701, Russia

Abstract: The structural mechanisms of formation of a hybrid-layered amorphous-nanocrystalline Cu/$Fe_{75}B_{17}Si_8$/Cu composite (crystalline copper as outer layers and amorphous $Fe_{75}B_{17}Si_8$ alloy as inner layer) upon deformation by high-pressure torsion (HPT) were investigated. Consolidation of the constructed composite was carried out by the HPT method at a degree of deformation corresponding to 1/4, 1, 5, 10, 20, and 25 revolutions. It was found that the hybrid composite consists of a strengthened copper matrix with embedded hard amorphous $Fe_{75}B_{17}Si_8$ phase fragments. The morphological features of the consolidation of a hybrid layered composite are associated with vortex instabilities of the deformation of material upon the HPT process. Because of the turbulence of the composite deformation, stresses arise on the irregularities of the hard phase layer, and, as a result, thin sites (bridges) appear in the layer of the amorphous $Fe_{75}B_{17}Si_8$ alloy. The ductile copper layers become thinner, and the initially rectangular cross-section of the hard amorphous $Fe_{75}B_{17}Si_8$ layer becomes "cigar-shaped" and bridges are formed in it. Further, with increasing degree of deformation, this layer becomes fragmented by breaking the bridges. The fragments are mixed with the matrix layer along the entire sample. The structure of the composite even after severe deformation by HPT is characterized by the absence of continuous interlayer boundaries.

Keywords: hybrid composite, high-pressure torsion, severe plastic deformation, layered structures, phase transformation

Acknowledgments: *The study was supported by the Russian Science Foundation, project #25-22-00132, https://rscf.ru/en/project/25-22-00132/.*

1. Introduction

It is known that amorphous-nanocrystalline composites can inherit the unique properties of the amorphous or nanocrystalline state, such as high magnetic softness, extraordinary wear and corrosion resistance, as well as high hardness and strength [1]. On the other hand, the amorphous-nanocrystalline composites are characterized by increased thermal stability and plasticity, which are hardly achieved by amorphous or nanocrystalline alloys separately. One of the directions for preparation of hybrid amorphous-nanocrystalline composites (along with the methods of controlled crystallization of amorphous alloys, mechanical activation, etc.) is the consolidation of freely laying alternating amorphous-crystalline layers by high-pressure torsion (HPT).

For example, the HPT method was used to consolidate two materials such as single-phase fcc CoCrFeMnNi and bcc HfNbTaTiZr high-entropy alloys [2, 3]. Upon HPT, vortex structures can be formed in layered composites due to the substantial deformation inhomogeneity typical of this deformation method [4]. The specific features of the vortex structure formation in Al/Cu and Al/Ni multilayer samples upon HPT deformation were studied in [5]. The possibility of the preparation of the layered amorphous-crystalline aluminum-based composites by the HPT method was examined in [6, 7]. For example, upon the consolidation of such composite, nanocrystallization processes with the precipitation of the Al phase begin in the amorphous part of the $Al_{86}Ni_9Gd_5$ ribbon and substantially increase the hardness of the alloy. Similar data were obtained in [6, 8] upon the consolidation of layered composites consisting of two amorphous $Al_{86}Ni_9Gd_5$ ribbons put between two multilayer aluminum foil stacks. The presence of several types of boundaries (transition regions) between dissimilar amorphous phases has been revealed in [9] upon the HPT consolidation of initially amorphous-nanocrystalline composite of two dissimilar $Ti_{50}Ni_{25}Cu_{25}$ and $Fe_{50}Ni_{33}B_{17}$ alloys. It has been experimentally shown that, in these composites, all observed types of transition regions (boundaries) between layers prevent noticeable mutual diffusion of elements between dissimilar layers. It is natural that the consolidation of layers by the HPT method is currently used for a wide range of composites [10–13]. Nevertheless, the structural features of freely laid, alternating amorphous-crystalline layers consolidated under HPT to date have been studied only fragmentarily. Therefore, the task of clarifying the general patterns of obtaining such composites under HPT conditions is very important and urgent. It is also reasonable to simultaneously identify the structural features of possible layer consolidation boundaries and the zones adjacent to them. In relation to the above, the aim of this work was to identify the structural features and mechanisms of deformation of the layered amorphous-crystalline Cu/FeSiB/Cu composite combining a high hardness of the amorphous layer and a high plasticity of the crystalline layer.

2. Experimental

Hybrid composites were prepared by stacking samples by a combination of amorphous and crystalline alloys, such as two technically pure crystalline copper ribbons and an amorphous $Fe_{75}B_{17}Si_8$ alloy ribbon between them. The consolidation of the constructed composite was carried out by the HPT method at a degree of deformation corresponding to (n) 1/4, 1, 5, 10, 20, and 25 revolutions of the movable anvil at a rotation velocity of 1 rpm under a quasi-hydrostatic pressure of 6 GPa in flat anvils. The diameter of the anvils was 8 mm. After completion of the deformation, the samples looked consolidated.

The amorphous $Fe_{75}B_{17}Si_8$ alloy was melted in a Balzers vacuum-induction furnace. Round rods with a diameter of 6–8 mm and a length of 300–400 mm were used as blanks for obtaining amorphous $Fe_{75}B_{17}Si_8$ ribbons by the melt spinning method. The rods were prepared by drawing the melt into quartz tubes. The melt temperature was not substantially higher than the solidification temperature of this alloy. Such requirements are caused by an intense development of porosity and oxidation with an increase in melt overheating. Then the rods were cut into pieces of about 50 g in weight. Stainless steel and copper with nickel and chromium coating were used as the material for the quenching disk for melt spinning. The nozzle slit width was 1.3 mm, the rotation velocity of the quenching disk was 2100 rpm, and the cooling rate was ≈10^6 K/s. The melt-spun amorphous $Fe_{75}B_{17}Si_8$ alloy ribbon was 10 mm wide and 20 μm thick.

Flat ingots of commercially pure Cu were prepared by casting. Then they were rolled and annealed at 500°C for 30 minutes in air to relieve internal stresses after rolling. The final thickness of the Cu strips was 100 μm.

Detailed studies of the structural-phase transformations and mechanical properties of the samples after HPT were carried out on transverse sections, except for the X-ray diffraction analysis using the external surfaces of the hybrid composite.

The structure of the hybrid composites and the distribution of chemical elements in their cross section were examined using a (SEM) Tescan Vega 3SBH scanning electron microscope with an electron microprobe analyzer in the backscattered electron mode at a magnification of ×500. The structure of the composite was studied in the center of the sample and in the middle of its radius.

The distribution of indentation hardness (H_{IT}) and indentation modulus (E_{IT}) across the cross-section of composite samples was measured with a NanoScan-3D automatic ultramicrotester at a load 10 g. The X-ray diffraction examination of the external surfaces of the composites (Cu crystalline layer) was performed with a DRON-3M diffractometer by the Bragg-Brentano method in a step-by-step mode in $Cu_{K\alpha}$ radiation using a graphite monochromator on a diffracted beam.

3. Results and discussion

The XRD patterns of the crystalline and amorphous layers are shown in Fig. 1.

As is seen in Fig. 1a, only two halos typical for the amorphous state are present in the X-ray diffraction pattern of the $Fe_{75}B_{17}Si_8$ alloy. Figure 1b represents the crystalline lines belonging only to the Cu phase. The broadening of the diffraction lines of the outer Cu layers of the composite during HPT was observed. The half-width of the $(113)_{Cu}$ line in the initial state was 0.373 ± 0.007. After HPT at $n = 25$, this same line had a half-width of 0.732 ± 0.018.

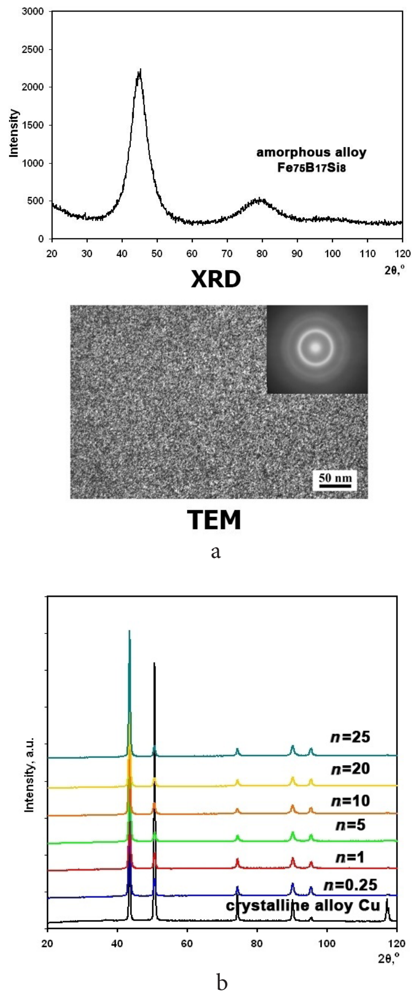

Fig. 1. (Color online) XRD patterns and typical dark-field TEM image of the initial state of the $Fe_{75}B_{17}Si_8$ amorphous layer (a) and Cu crystalline layer in the initial state and after HPT (b).

The SEM images of the cross-sections of the Cu/FeSiB/Cu composite after HPT show a consolidated material (Fig. 2). The fragments of the hard amorphous $Fe_{75}B_{17}Si_8$ phase (of 8.8 GPa in the initial hardness) are distributed along the entire sample against the background of the copper matrix (of 0.9 GPa in the initial hardness). The fragments are usually "cigar-shaped" with bridges (Fig. 2a). After HPT deformation to small degrees, from $n=1/4$ to $n=1$, the fragment length varies between ≈50 and 400 μm.

Similar "cigar-shaped" fragments of a small size are also present after HPT to $n=25$ (Fig. 2b). As a rule, it is impossible to detect any continuous boundary between the copper matrix and fragments of the amorphous $Fe_{75}B_{17}Si_8$ phase. There is a gap everywhere between the layers, and its width decreases with increasing degree of deformation. Upon HPT, the gap between the copper matrix and the amorphous $Fe_{75}B_{17}Si_8$ phase decreases from ≈4 μm to ≈0.5 μm with increasing number of revolutions from $n=1$ to $n=25$. Note that even the smallest fragments of the amorphous $Fe_{75}B_{17}Si_8$ alloy exhibit gaps with the matrix up to severe deformation (Fig. 3).

The chemical composition of the crystalline copper matrix and the amorphous $Fe_{75}B_{17}Si_8$ alloy consolidated in it remains unchanged at all degrees of deformation. For example, Fig. 3 shows a consolidated fragment of the amorphous $Fe_{75}B_{17}Si_8$ phase in a copper matrix after HPT to $n=25$. It is seen that the chemical composition of the composite layers has not changed.

The indentation hardness (H_{IT}) and indentation modulus (E_{IT}) of different composite layers were measured both in the initial state and after HPT (Fig. 4). It is shown that H_{IT} of the copper layer of the composite increases upon deformation and reaches saturation after HPT to $n=5$. The increase in H_{IT} is associated with a decrease in the grain size in the copper layer and the accumulation of the density of deformation defects [14] upon HPT. The increase in the half-widths of the diffraction maxima in the X-ray patterns by HPT also confirms the deformation of the copper layers of the composite (Fig. 1). The amorphous $Fe_{75}B_{17}Si_8$ layer with increasing degree of deformation exhibits virtually constant H_{IT} and E_{IT} levels within the measurement error.

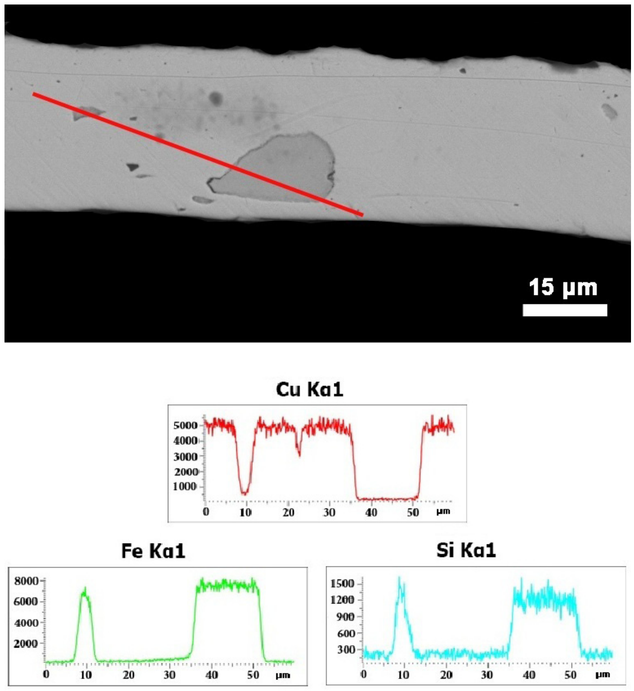

Fig. 3. (Color online) SEM image of a fragment of the hard phase and changes in the chemical composition along the analysis line of the composite after HPT to $n=25$.

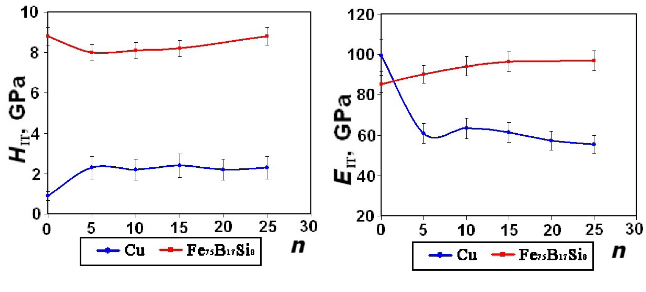

a b

Fig. 4. (Color online) Dependence of H_{IT} (a) and E_{IT} (b) on the number of revolutions n for the Cu and $Fe_{75}B_{17}Si_8$ layers.

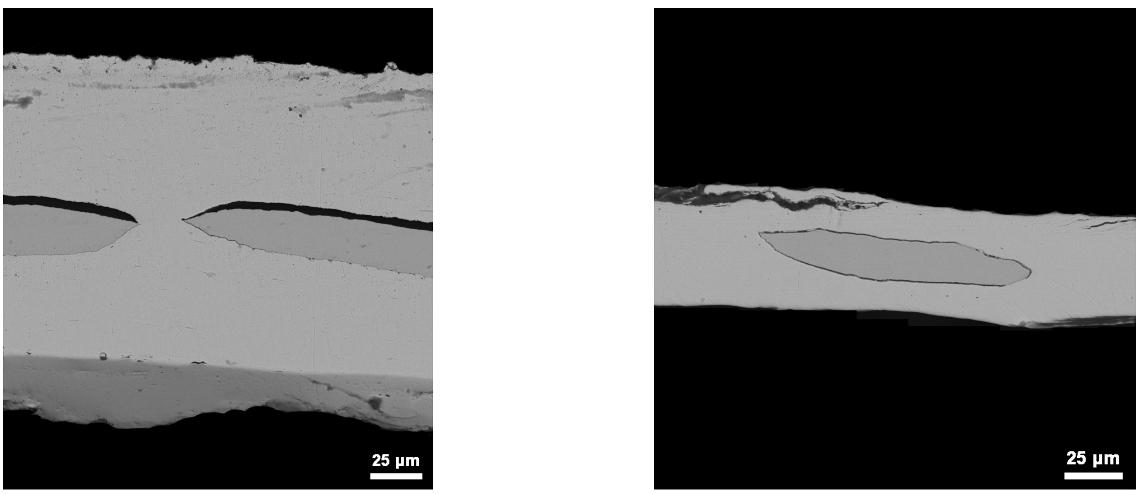

a b

Fig. 2. SEM images of the cross-sectional structure of the composite after HPT: $n=1$ (a) and $n=25$ (b).

Observing the changes in the shape and size of fragments of the hard $Fe_{75}B_{17}Si_8$ amorphous phase, we can imagine a step-by-step mechanism of its refinement. The most informative data were obtained from the composite structure evolution at the middle of the sample radius. Already after HPT to $n=1/4$, the transverse section of the hybrid composite exhibits (Fig. 5) that the layer of the hard amorphous $Fe_{75}B_{17}Si_8$ phase was disintegrated into fragments, which are located along the entire sample. The fragments are "cigar-shaped" with sharp ends. The longest fragments have bridges. Further refinement of the amorphous $Fe_{75}B_{17}Si_8$ layer is associated with the rupture of the bridges and the destruction (refinement) of the fragments. The soft and very ductile copper matrix (Fig. 4), becomes thinner, envelops the layer of the amorphous $Fe_{75}B_{17}Si_8$ phase and transmits deformation to this layer. The harder amorphous $Fe_{75}B_{17}Si_8$ layer with low plasticity (Fig. 4) is destroyed and disintegrated into primary fragments. The copper matrix envelops the resulting primary fragments. With increasing degree of deformation, the process of crushing the primary fragments is reproduced many times.

The stages of the structure evolution on the hybrid amorphous-crystalline composite with increasing degree of deformation by HPT are schematically shown in Fig. 5.

1. Deformation (thinning and refinement) of the copper layer of the composite with the simultaneous formation of bridges in the layer of the amorphous $Fe_{75}B_{17}Si_8$ phase under the effect of HPT.

2. Breakdown of bridges and the beginning of the refinement of the hard $Fe_{75}B_{17}Si_8$ amorphous phase.

3. Mixing and distribution of the hard $Fe_{75}B_{17}Si_8$ phase fragments along the sample. The gap between soft copper and the hard amorphous $Fe_{75}B_{17}Si_8$ phase is saved up to the highest degrees of deformation because of the lack of affinity between the atoms of the main chemical components of the original layers and the difference in the atomic structure of the layers under study.

It is known that the individual layers constituting the hybrid composite under study differ in deformation behavior upon HPT under similar conditions. For example, copper taken separately is refined and strengthened [14]. An isolated amorphous $Fe_{75}B_{17}Si_8$ alloy is nanocrystallized upon HPT already to $n=1$ [15]. In the present study, the final composite consists of a fine-crystalline [14] and strengthened copper matrix (Fig. 4) with embedded fragments of the hard $Fe_{75}B_{17}Si_8$ amorphous phase. That is, the copper matrix is strengthened and refined, but the gap between the matrix and the $Fe_{75}B_{17}Si_8$ amorphous phase, as noted above, is retained up to $n=25$ (Fig. 2). The presence of a gap between the layers of the hybrid composite can be explained as follows. First, as follows from the Fe-Cu phase diagram [16], the mutual solubility between Fe and Cu at room temperature is chemically impossible, and, second, mixing can also be hindered by a significant difference in the mechanical properties and atomic structures of the composite layers of crystalline copper and the amorphous $Fe_{75}B_{17}Si_8$ phase. Note that a three-layer composite consisting of the amorphous $Fe_{50}Ni_{33}B_{17}$ alloy between two crystalline $Ti_{50}Ni_{25}Cu_{25}$ alloy layers after HPT exhibited mainly consolidated boundaries between the layers [8]. Consequently, the occurrence and retention of the gaps between the layers in our case is most likely explained by the impossibility of the room-temperature interaction between the main components of the layers under study.

The preparation of hybrid composites from samples of various configurations at room temperature has been investigated in a number of works [17–23]. The characteristic features of changes in the structure of layered composites after HPT in the present work generally correlate with the above-mentioned literature data. The deformation rates of the layers in the composite upon HPT substantially differ because of a great difference between their mechanical properties (Fig. 4). The deformation of the entire sample enters a turbulent stage. Because of the turbulence of the composite deformation, stresses arise on the irregularities of the hard phase layer, and, as a result, thin sites (bridges) appear in the layer of the amorphous $Fe_{75}B_{17}Si_8$ alloy. The ductile copper layers become thinner, and the initially rectangular cross-section of the hard amorphous $Fe_{75}B_{17}Si_8$ layer becomes "cigar-shaped",

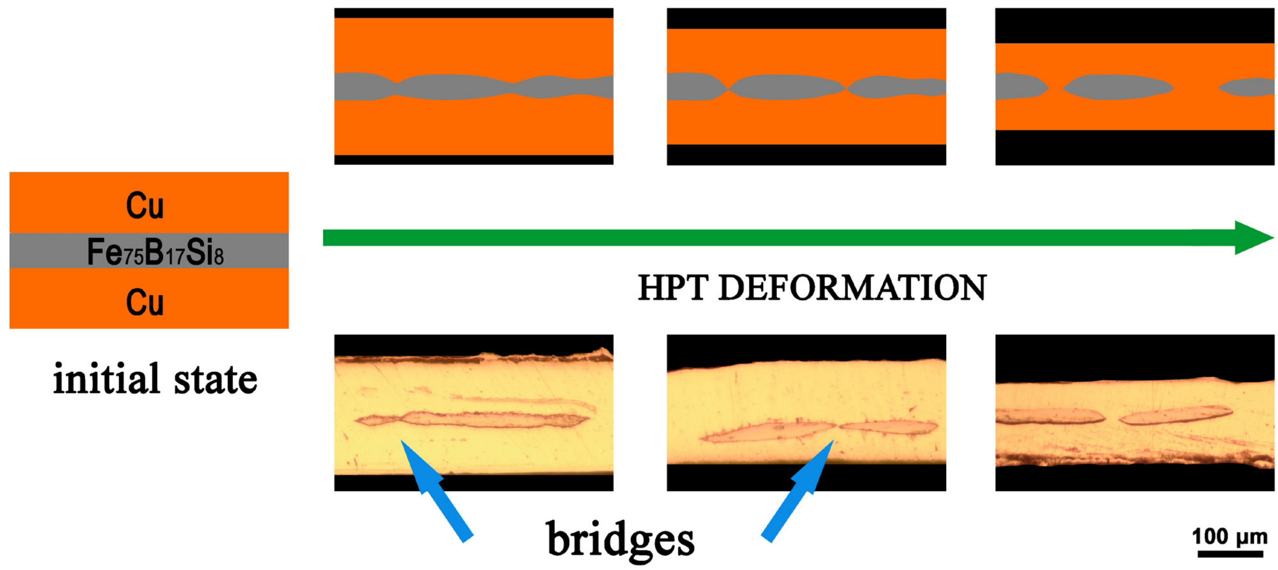

Fig. 5. (Color online) Optical-microscopic images of the Cu/FeSiB/Cu composite structure and scheme of its change upon HPT.

and, as is mentioned above, bridges are formed in it. Further, with increasing degree of deformation, this layer becomes fragmented by breaking the bridges. The fragments are mixed with the matrix layer along the entire sample. In this study, no crystallization of the amorphous $Fe_{75}B_{17}Si_8$ layer was recorded upon HPT [8]. The fragment size, as a rule, decreases from the center to the edge of the composite sample. Hard fragments of the amorphous $Fe_{75}B_{17}Si_8$ phase become obstacles to the development of plastic deformation of the softer copper matrix. Some researchers [5,24] believe that the vortices of metal layers observed upon HPT in layered composites consisting of dissimilar layers are caused by instabilities in plastic deformation at the expense of local blocking of shear deformation in ductile layers.

4. Conclusion

The structure evolution of the layered amorphous-crystalline Cu/FeSiB/Cu composite subjected to HPT at room temperature has been examined by various structural methods. The composite combines the high hardness of the amorphous $Fe_{75}B_{17}Si_8$ phase and the plasticity of the crystalline copper layers. Under the effect of HPT, the copper component of the composite becomes thinner. Simultaneous thinning of the hard amorphous $Fe_{75}B_{17}Si_8$ phase layer is accompanied by the formation of bridges in it. With increasing degree of deformation, the bridges break, the $Fe_{75}B_{17}Si_8$ amorphous phase is refined, and the hard phase fragments are mixed and distributed along the sample. As a result, the final material consists of a strengthened copper matrix with fragments of the hard amorphous $Fe_{75}B_{17}Si_8$ phase embedded in it. It is assumed that the observed effects are associated with vortex instabilities of deformation in ductile copper layers under the effect of local braking of shear deformation by fragments of the hard amorphous $Fe_{75}B_{17}Si_8$ phase. The structure of the composite even after severe deformation by HPT is characterized by the absence of continuous interlayer boundaries.

Conflicts of interest: *The authors declare that they have no known competing financial interests or personal relationships that could have appeared to influence the work reported in this paper.*

Data and code availability: *The authors are unable or have chosen not to specify which data has been used.*

References

1. F.C. Li, T. Liu, J.Y. Zhang, S. Shuang, Q. Wang, A.D. Wang, J.G. Wang, Y. Yang, Amorphous-nanocrystalline alloys: fabrication, properties, and applications, Materials Today Advances 4 (2019) 100027.
2. J. Li, H. Chen, H. Feng, Q. Fang, Y. Liu, F. Liu, H. Wu, P.K. Liaw, Microstructure evolution and deformation mechanism of amorphous/crystalline high-entropy-alloy composites, Journal of Materials Science & Technology 54 (2020) 14–19.
3. S. Taheriniya, F.A. Davani, S. Hilke, M. Hepp, C. Gadelmeier, M.R. Chellali, T. Boll, H. Rösner, M. Peterlechner, C. Gammer, S.V. Divinski, B. Butz, U. Glatzel, H. Hahn, G. Wilde, High entropy alloy nanocomposites produced by high pressure torsion, Acta Mater. 208 (2021) 116714.
4. A.M. Glezer, R.V. Sundeev, A.V. Shalimova, L.S. Metlov, Physics of severe plastic deformation, Phys. Usp. 66 (2023) 32–58.
5. R. Kulagin, Y. Beygelzimer, Yu. Ivanisenko, A. Mazilkin, B. Straumal, H. Hahn, Instabilities of interfaces between dissimilar metals induced by high pressure torsion, Mater. Lett. 222 (2018) 172–175.
6. S.V. Vasiliev, A.I. Limanovskii, V.M. Tkachenko, T.V. Tsvetkov, K.A. Svyrydova, V.V. Burkhovetskii, V.I. Tkatch, Amorphous-crystalline Al-based laminates with enhanced plasticity produced by high pressure torsion, Mater. Lett. 318 (2022) 132155.
7. S.V. Vasiliev, A.I. Limanovskii, V.M. Tkachenko, T.V. Tsvetkov, K.A. Svyrydova, V.V. Burkhovetskii, V.N. Sayapin, S.V. Terekhov, V.I. Tkatch, Fabrication of consolidated layered samples by high-pressure torsion processing of rapidly solidified Al-based ribbons with amorphous and crystalline structures, Materials Today Communications 24 (2020) 101080.
8. R. Sundeev, A. Shalimova, S. Rogachev, O. Chernogorova, A. Glezer, A. Ovcharov, I. Karateev, N. Tabachkova, Structural Aspects of the Formation of Multilayer Composites from Dissimilar Materials upon High-Pressure Torsion, Materials 16 (2023) 3849.
9. E.H. Ekiz, T.G. Lach, R.S. Averback, N.A. Mara, I.J. Beyerlein, M. Pouryazdan, H. Hahn, P. Bellon, Microstructural evolution of nanolayered Cu-Nb composites subjected to high-pressure torsion, Acta Mater. 72 (2014) 178–191.
10. V.N. Danilenko, S.N. Sergeev, J.A. Baimova, G.F. Korznikova, K.S. Nazarov, R.Kh. Khisamov, A.M. Glezer, R.R. Mulyukov, An approach for fabrication of Al-Cu composite by high pressure torsion, Mater. Lett. 236 (2019) 51–55.
11. G.F. Korznikova, K.S. Nazarov, R.Kh. Khisamov, S.N. Sergeev, R.U. Shayachmetov, G.R. Khalikova, J.A. Baimova, A.M. Glezer, R.R. Mulyukov, Intermetallic growth kinetics and microstructure evolution in Al-Cu-Al metal-matrix composite processed by high pressure torsion, Mater. Lett. 253 (2019) 412–415.
12. P. Bazarnik, A. Bartkowska, B, Romelczyk-Baishya, B. Adamczyk-Cieślak, J. Dai, Y. Huang, M. Lewandowska, T.G. Langdon, Superior strength of tri-layered Al-Cu-Al nano-composites processed by high-pressure torsion, Journal of Alloys and Compounds 846 (2020) 156380.
13. Y. Ivanisenko, A. Mazilkin, I. Gallino, S.S. Riegler, S. Doyle, A. Kilmametov, O. Fabrichnay, M. Heilmaier, On the formation of nanocrystalline aluminides during high pressure torsion of Al/Ni alternating foils and post-processing multilayer reaction, Journal of Alloys and Compounds 905 (2022) 164201.
14. X.H. An, S.D. Wu, Z.F. Zhang, R.B. Figueiredo, N. Gao, T.G. Langdon, Evolution of microstructural homogeneity in copper processed by high-pressure torsion, Scripta Materialia 63 (2010) 560–563.
15. R.V. Sundeev, A.M. Glezer, A.P. Menushenkov, A.V. Shalimova, O.V. Chernysheva, N.V. Umnova, Effect of

high pressure torsion at different temperatures on the local atomic structure of amorphous Fe-Ni-B alloys, Materials and Design 135 (2017) 77–83.
16. L. Son, V. Sidorov, N. Katkov Statistics and Thermodynamics of Fe-Cu Alloys at High Temperatures, EPJ Web of Conferences 151 (2017) 05003.
17. M.M. Castro, S. Sabbaghianrad, P. Henriqu, R. Pereira, E.M. Mazzer, A. Isaac, T.G. Langdon, R.B. Figueiredo, A magnesium-aluminium composite produced by high-pressure torsion, Journal of Alloys and Compounds, 804 (2019) 421–426.
18. S.O. Rogachev, S.A. Nikulin, V.M. Khatkevich, R.V. Sundeev, A.A. Komissarov, Features of structure formation in layered metallic materials processed by high pressure torsion, Metallurgical and Materials Transactions A 51 (2020) 1781–1788.
19. P. Bazarnik, A. Bartkowska, Y. Huang, K. Szlązak, B. Adamczyk-Cieślak, J. Sort, M. Lewandowska, T.G. Langdon, Fabrication of hybrid nanocrystalline Al-Ti alloys by mechanical bonding through high-pressure torsion, Materials Science and Engineering: A 833 (2022) 142549.
20. X. Chen, L. Xiao, Y. Liu, M. Xu, T. Xu, B Gao, Z. Hu, H. Zhou, High strength-ductility of heterogeneous sandwich Mg-Y alloys produced by high pressure torsion, Vacuum 179 (2020) 109568.
21. M.M. Yashin, V.E. Ryabukhin, A.N. Yurasov, Magneto-optical transverse Kerr effect in $Co_x(CoO)_{1-x}$ nanocomposites, Russian Technological Journal 13 (1) (2025) 115–121.
22. V. Tavakkoli, A. Mazilkin, T. Scherer, M. Mail, Y. Beygelzimer, B. Baretzky, Y. Estrin, R. Kulagin, Instability of a molybdenum layer under deformation of a CuMoCu laminate by high-pressure torsion, Mater. Lett. 302 (2021) 130378.
23. S.O. Rogachev, V.M. Khatkevich, R.V. Sundeev, High strength in layered metal composites obtained by high-pressure torsion, Mater. Lett. 303 (2021) 130567.
24. A. Mazilkin, V. Tavakkoli, O. Davydenko, Y. Beygelzimer, E. Boltynjuk, T. Boll, B. Straumal, B. Baretzky, Y. Estrin, R. Kulagin, Mechanisms of structural evolution of laminates with immiscible components under high-pressure torsion, Acta Materialia 269 (2024) 119804.